HHS Public Access

Author manuscript

Magn Reson Imaging. Author manuscript; available in PMC 2019 September 01.

Published in final edited form as:

Magn Reson Imaging. 2018 September ; 51: 173–181. doi:10.1016/j.mri.2018.04.006.

Quantitative Diffusion MRI using Reduced Field-of-View and Multi-Shot Acquisition Techniques: Validation in Phantoms and Prostate Imaging

Yuxin Zhang, BS.[1,2], **James Holmes, PhD.**[2], **Iñaki Rabanillo, MS.**[3], **Arnaud Guidon, PhD.**[4], **Shane Wells, MD.**[2], and **Diego Hernando, PhD.**[1,2]

[1]Department of Medical Physics, University of Wisconsin Madison, Madison, WI, United States

[2]Department of Radiology, School of Medicine and Public Health, University of Wisconsin Madison, Madison, WI, United States

[3]Laboratorio MR de Procesado de Imagen, Universidad de Valladolid, Valladolid, Spain

[4]Applications and Workflow, GE Healthcare, Boston, MA, United States

Abstract

Purpose—To evaluate the reproducibility of quantitative diffusion measurements obtained with reduced Field of View (rFOV) and Multi-shot EPI (msEPI) acquisitions, using single-shot EPI (ssEPI) as a reference.

Methods—Diffusion phantom experiments, and prostate diffusion-weighted imaging in healthy volunteers and patients with known or suspected prostate cancer were performed across the three different sequences. Quantitative diffusion measurements of apparent diffusion coefficient, and diffusion kurtosis parameters (healthy volunteers), were obtained and compared across diffusion sequences (rFOV, msEPI, and ssEPI). Other possible confounding factors like b-value combinations and acquisition parameters were also investigated.

Results—Both msEPI and rFOV have shown reproducible quantitative diffusion measurements relative to ssEPI; no significant difference in ADC was observed across pulse sequences in the standard diffusion phantom ($p=0.156$), healthy volunteers ($p\geq0.12$) or patients ($p\geq0.26$). The ADC values within the non-cancerous central gland and peripheral zone of patients were $1.29\pm0.17\times10^{-3}$ mm^2/s and $1.74\pm0.23\times10^{-3}$ mm^2/s respectively. However, differences in quantitative diffusion parameters were observed across different number of averages for rFOV, and across b-value groups and diffusion models for all the three sequences.

Conclusion—Both rFOV and msEPI have the potential to provide high image quality with reproducible quantitative diffusion measurements in prostate diffusion MRI.

*Corresponding author: Diego Hernando, Departments of Radiology and Medical Physics, University of Wisconsin-Madison, Madison, WI 53705 USA, dhernando@wisc.edu.

Keywords

Quantitative diffusion MRI; prostate imaging; reduced Field-of-View; Multi-Shot EPI

1. Introduction

Diffusion MRI provides a powerful non-invasive probe of tissue microstructure, with multiple important applications in the assessment of healthy and diseased tissue. Diffusion MRI techniques include both qualitative diffusion-weighted imaging (DWI) and quantitative diffusion techniques [1]. Quantitative diffusion MRI techniques are based on acquiring multiple DW images with different diffusion weightings, and performing parametric fitting of the acquired signal in order to estimate quantitative diffusion parameters of tissue [2, 3].

Prostate imaging is an important application of diffusion MRI. Prostate cancer is the second most frequently diagnosed cancer among men worldwide [4, 5], and there is a broad clinical need for techniques that enable diagnosis, staging and treatment monitoring of prostate cancer [6, 7]. Qualitative DWI is widely used in the clinic for the assessment of prostate cancer and other prostatic diseases, and is included in the PI-RADS guidelines [8].

Prostate DWI is typically performed with single-shot echo planar imaging (ssEPI) techniques, due to their reliability and robustness to motion. Importantly, ssEPI based DWI has been demonstrated to show significant contrast between malignant and benign peripheral zone tissues [9–11]. However, ssEPI of the prostate often suffers from severe image distortion due to the presence of susceptibility-related field inhomogeneity. The prostate is located directly under the bladder and in front of the rectum. This complicated anatomic environment including abrupt susceptibility differences between prostate tissue and the air in the rectum will result in severe field inhomogeneity. This field inhomogeneity introduces significant distortion in ssEPI images, which are obtained over a long readout time. This distortion in ssEPI-DWI results in reduced image quality and poor co-localization with other imaging sequences, and may complicate the accurate measurement of quantitative diffusion parameters within and around the prostate.

Novel pulse sequences based on reduced field-of-view (rFOV) [14, 28–31] and multi-shot EPI (msEPI) [15–17] acquisitions have been proposed to reduce these image distortions by enabling shorter readout times. Specifically, rFOV enables a shorter EPI echo-train length by applying a spatially-selective RF pulse to excite a limited FOV in the phase encoding direction. Alternatively, msEPI acquires multiple shots (where each shot requires a shorter echo train with reduced readout time) in the phase-encoding direction to reduce distortion artifacts. Importantly, both rFOV and msEPI enable DWI imaging with higher resolution and higher overall image quality including greater resolvable spatial resolution and reduced distortions [14, 17]. In recent studies, both rFOV and msEPI have been shown to provide improved diffusion-weighted image quality for prostate cancer detection compared to conventional ssEPI [18–20, 35–39].

Quantitative diffusion measurements (such as ADC) have tremendous potential to enable improved detection and staging of prostate cancer and assessment of response to treatment

[9–12]. Based on these quantitative measurements, thresholds have been obtained that enable staging of lesions [32] as well as early assessment of response to treatment [33, 34] of prostate cancer and its metastases. However, the quantitative reproducibility of rFOV and msEPI relative to ssEPI has not been demonstrated. Consequently, establishing this reproducibility is essential to determine whether previously derived thresholds (obtained from ssEPI studies) can be used with rFOV or msEPI, as well as to ensure data harmonization in multi-site clinical trials (where different sites may use different diffusion pulse sequences). Although preliminary studies suggest that rFOV and msEPI are able to produce accurate ADC measurements in quantitative diffusion phantoms [21, 22], the reproducibility of quantitative diffusion measurements obtained from these novel diffusion MRI sequences has not been demonstrated.

Furthermore, in-vivo tissue often has restricted diffusion, which induces bias in ADC measurements with different b-value combinations [13, 44]. Diffusion kurtosis model has been introduced to measure restricted diffusion [3, 4] independently from b-value choices. Previous studies have examined kurtosis imaging in the prostate [12, 41–43]. But similarly, the reproducibility of quantitative diffusion measurements with different b-value combinations and with kurtosis model also need to be evaluated with novel imaging acquisition strategies like rFOV and msEPI.

Therefore, the overall purpose of this study was to evaluate the reproducibility of quantitative diffusion measurements obtained with rFOV and msEPI acquisitions, using ssEPI as a reference. Additionally, the reproducibility across the choice of b-value combination and other acquisition parameters were also evaluated. This paper is aimed to constitute an early-stage technical validation towards further clinical evaluation.

2. Methods

To investigate the reproducibility of quantitative diffusion measurements from rFOV and msEPI acquisitions relative to ssEPI, diffusion phantom experiments, prostate imaging in healthy volunteers and prostate imaging in clinical patients were conducted. In addition, different acquisition parameters and quantitative diffusion models were used for further evaluation of reproducibility across these confounding factors. Experimental details are described in the following sections.

2.1 Diffusion phantom experiments

A National Institute of Standards and Technology (NIST) and RSNA-QIBA diffusion phantom [23], containing multiple vials with different ADC, was used to evaluate three different diffusion sequences across acquisition parameters. The diffusion phantom was scanned using a 3T 60cm bore scanner (MR 750, GE Healthcare, Waukesha, WI). To reduce thermal changes in ADC, the temperature of the phantom was controlled at 0°C using an ice-water bath. The phantom was placed into an eight-channel head coil, with the vials aligned parallel to the magnetic field. Axial ssEPI DW images were acquired with parallel imaging factor = 2 as the reference. rFOV and four-shot msEPI sequences were acquired several times with different imaging parameters. Resolution for different sequence was

slightly different based on their image quality. Detailed imaging parameters are provided in Table 1.

The acquired diffusion-weighted images were reconstructed for each acquisition (note that multi-shot acquisitions in msEPI were reconstructed using a generalized parallel imaging reconstruction method described in Ref. [17]). ADC maps were then calculated for each acquisition, by fitting a mono-exponential diffusion model to the voxel-wise signal using non-linear least-squares fitting. For each protocol, averaged ADC measurements were performed within an approximately 1cm^2 region-of-interest (ROI) within each vial. ANCOVA [24] analysis was conducted across different diffusion imaging sequences, using the different phantom vials as the covariate.

2.2 Volunteer study in the prostate

This HIPAA-compliant study including healthy volunteers and patients was performed with institutional review board approval and informed written consent.

2.2.1 Healthy volunteers—Ten healthy volunteers (29±7 years of age) were scanned with a 32-channel receive only Torso coil (GE healthcare, Waukesha, WI) on a 60cm bore 3T scanner (GE healthcare, Waukesha, WI) to evaluate the image quality, quantitative diffusion reproducibility among the three sequences. The three diffusion imaging sequences were performed as described in Table 2. All three diffusion directions are acquired for each sequence. Specifically, ssEPI was conducted with a parallel imaging acceleration factor of two; while msEPI images were acquired with four shots and reconstructed with a generalized parallel imaging technique [17]. Reduction factor of rFOV in the phase encoding direction (R/L) was 40%. Due to the longer acquisition time of multiple shots, msEPI acquisitions were performed with higher spatial resolution than ssEPI and rFOV to achieve similar SNR.

To further evaluate the quantitative measurements across different b-value combinations under restricted diffusion of prostate tissue, two b-value groups, each with seven b-values (Table 2(b)), were acquired under the same acquisition parameters. In the high b-value group, b values are from 10 s/mm^2 up to 1500 s/mm^2; whereas the low b-value group has b-value up to 800 s/mm^2. The maximum b-value in each group was chosen based on the clinical protocol for prostate DWI, but more b-values were acquired to obtain more accurate quantitative fitting. Quantitative diffusion maps were calculated using the following two different diffusion models:

1. Mono-exponential diffusion model:

$$S(b) = S_0 e^{-bADC_m}; \quad (1)$$

2. Kurtosis model [3, 4]:

$$S(b) = S_0 e^{-bD_k + \frac{1}{6}b^2 D_k^2 k}; \quad (2)$$

where S(b) is the signal intensity for a specific b-value, S_0 is the signal intensity at b=0 s/mm^2. ADC and D_k are the diffusion coefficients for the two models, respectively; k is kurtosis.

In addition to the diffusion imaging sequences, a T2-weighted 2D multi-slice Fast Spin Echo (FSE) acquisition with axial slices co-localized with the diffusion imaging slices was acquired. Specific imaging parameters included: FOV=28cmx28cm, slice thickness=5mm, in-plane spatial resolution=0.875mmx0.786mm, TE=98.4ms, TR=3.4s, echo train length=23, readout bandwidth= 50kHz, acquisition time=3min14s and flip angle=111°. This non-EPI T2-weighted acquisition was used as a reference to assess the geometric distortions present in each of the diffusion imaging sequences. In order to evaluate geometric distortions, the diameter of the prostate in the A/P and R/L directions was measured from axial diffusion-weighted images (ssEPI, rFOV and msEPI). These measurements were compared to those from the non-EPI T2-weighted acquisition, which was used as reference [36]. The distortion present in ssEPI, rFOV and msEPI was compared by analyzing the averaged diameter differences using a one-tail t-test.

To assess the reproducibility of the diffusion measurements for each of the two signal models, pair-wise Bland-Altman analysis [40] was performed across different pulse sequences (rFOV vs. ssEPI and msEPI vs. ssEPI) and different b-value groups (high b-value group vs. low b-value group). Averaged diffusion measurements (ADC and D_k) within an approximately 0.6cm^2 central gland (CG) ROI and an approximately 0.8cm^2 peripheral zone (PZ) ROI were compared for each volunteer in the analysis. ROIs were selected by avoiding distorted regions where ssEPI measurements were used as a reference. The ROIs were co-localized for different imaging sequences.

2.2.2 Clinical patients—Four clinical patients (61±5 years old) undergoing prostate MRI were recruited for this study, each with 12 diffusion measurements at different areas. Images were acquired according to the University of Wisconsin clinical prostate protocol and before contrast agent administration, using a 30-channel cardiac coil array (GE healthcare, Waukesha, WI) on a 3T scanner (GE healthcare, Waukesha, WI). The detailed protocol is listed in Table 2(b). In these patients, four DWI sequences, including ssEPI, rFOV$_s$, rFOV$_l$ and msEPI (where rFOV$_s$ was a short acquisition with few averages and rFOV$_l$ was a longer acquisition with more averages), were scanned with the same b-values (b= [100, 800] s/mm^2) as in the clinical DWI sequences. Antiperistatic agents were not applied to these patients in the research sequences. All three diffusion directions were acquired for each sequence. Reduction factor of rFOV was 50% performed with the phase encoding direction (R/L or A/P) chosen to minimize susceptibility related artifacts for each patient. Due to the limited patient scan time, only a small number of averages were used in each of the ssEPI, rFOV$_s$ and msEPI sequences. But to further compare the diffusion measurements of rFOV with different number of averages, rFOV$_l$ with a larger number of averages was also

acquired and analyzed. msEPI acquisitions were performed with higher spatial resolution than ssEPI and rFOV because it has multiple shots.

Because of the limited range of b-values obtained in patients, only ADC maps from a mono-exponential diffusion model were reconstructed from patient images. From the resulting ADC maps, eight ROIs were selected for each patient, including left and right PZ on apex, left and right central gland (CG) on apex plane, left and right PZ on mid plane, and left and right CG on mid plane. Among the ROIs, cancerous PZ regions were excluded. In order to assess the reproducibility of quantitative diffusion imaging using different pulse sequences, Bland-Altman analysis was conducted to compare these ROI-based ADC measurements across different sequences ($rFOV_s$ versus ssEPI, msEPI versus ssEPI, and $rFOV_l$ versus ssEPI).

Image post-processing and analysis in this study was performed in MATLAB (R2016a, The Mathworks Inc.). Multivariate statistical analysis was implemented with IBM SPSS (IBM Corporation, Armonk, New York) V23.0.

3. Results

Figure 1 shows representative diffusion-weighted images and ADC maps across three sequences acquired in the diffusion phantom. ssEPI images show distortion (Black arrows) where the vials have a circular cross-section. Both rFOV and msEPI acquisitions reduce the geometric distortion.

Overall, ADC measurements from both rFOV and msEPI are in good agreement ($R^2 > 0.99$) with the reference ssEPI as shown in Fig. 2. Different slice thickness and resolution does not have a large effect on ADC measurements from either rFOV or msEPI. However, rFOV slightly underestimated ADC with thinner slice and smaller number of averages.

Multivariate analysis of the phantom measurements demonstrates no significant effect ($P>0.05$, effect size $\eta^2 <0.02$) of different sequences ($F=1.868$, $P=0.156$, partial $\eta^2 =0.008$), even with different acquisition parameters.

Diffusion-weighted images and ADC maps of the prostate of a healthy young volunteer are presented in Fig. 3. Distortions within the prostate are improved in rFOV and msEPI (white arrows). Note that rFOV depicts only a limited FOV with lower SNR. The quantified image distortion for each pulse sequence is shown in Fig. 4. Mean values and standard deviations of the diameter differences relative to the non-EPI T2-weighted imaging reference in R/L and A/P directions are plotted. P-values from the t-test are shown adjacent to each bar. Significantly lower distortion ($P<0.05$) in the A/P direction is demonstrated for both rFOV and msEPI.

Quantitative diffusion measurements of peripheral zone (PZ) and central gland (CG) with each combination of sequence, b-value group and diffusion model are listed in Table 3(a). Table 4 shows the Bland-Altman analysis of volunteer data across the three pulse sequences (a) and different b-value groups (b) with both mono-exponential model and kurtosis model. According to the bias results, no significant difference ($p>0.05$) has been shown across

sequences, even though the in- plane resolution is different for msEPI; but significant bias of ADC estimations exists across b-value groups ($p<0.01$). From the width of the 95% confidence interval ($\pm 1.96\sigma$, where σ is the standard deviation of the difference between the quantitative measurements from different sequences) [40], both rFOV and msEPI have moderate confidence intervals ($1.96\sigma < 0.3\times10^{-6}$ mm^2/s) relative to ssEPI ADC measurements from a mono-exponential model. However, the confidence intervals for both rFOV and msEPI relative to ssEPI are larger for the parameter D_k measured from the diffusion kurtosis model.

ADC measurements from patients are shown in Table 3(b). The results of Bland-Altman analysis across sequences are plotted in Fig. 5. There is no significant difference between msEPI and ssEPI ($p=0.32$) and between $rFOV_1$ and ssEPI ($p=0.26$). But a 0.1×10^{-3} mm^2/s bias is observed between $rFOV_s$ and ssEPI with $p<0.01$.

4. Discussion

As an initial step towards further clinical studies, this study evaluated the reproducibility of quantitative diffusion measurements across different pulse sequences (ssEPI, rFOV and msEPI) in phantoms and prostate of healthy volunteers and clinical patients. From our results, quantitative diffusion measurements obtained from recently developed reduced-distortion pulse sequences (rFOV and msEPI) were in good agreement with the standard ssEPI-based measurements. In combination with the reduced distortion provided by these novel pulse sequences (as has been demonstrated in previous works [18–20, 35–39] as well as in this study), these results demonstrate the potential of rFOV and msEPI, at the cost of FOV size or scan time, to provide reproducible quantitative diffusion measurements compared to ssEPI. This potential may have significant research and clinical implications for diffusion MRI of the prostate.

rFOV is able to reduce distortion in diffusion-weighted images through limiting the size of the FOV. In this work, both phantom experiments and volunteer studies have shown no significant difference ($p>0.05$) in quantitative diffusion measurements between rFOV and ssEPI. This agrees with the conclusions from other evaluation studies [22]. However, it has been demonstrated that rFOV images tend to have lower SNR especially when the average number is small and b-value is high [29]. This property will induce an underestimation in quantitative diffusion measurements, which can be fixed by using larger number of averages and choosing optimal b-values [22]. In this work, it is shown from both phantom and patient studies that diffusion measurements of rFOV with larger number of averages have less bias than those with small number of averages.

msEPI has the capability for high resolution diffusion-weighted images with less distortion than ssEPI and without sacrificing scan coverage by reducing the FOV [20]. Overall, ADC measurements from msEPI have no significant difference from ssEPI and rFOV based on both multivariate analysis of the phantom data and Bland-Altman analysis of volunteer studies shown in the results section. In principle, residual parallel imaging artifacts from the current implementation of msEPI reconstruction may increase the variability of msEPI-

derived quantitative measurements, however no systematic bias was observed relative to ssEPI measurements.

Additionally, for all the three sequences, the choice of b-values and diffusion models will affect the quantitative diffusion measurements [12, 13]. Previous studies have demonstrated significant difference of diffusion measurements between different combinations of b-values in both healthy and cancerous prostate tissues [13]. This difference may be induced by several causes, including the presence of perfusion or pseudo-diffusion effects at low b-values, as well as restricted diffusion and potentially noise floor effects at high b-values [26, 27]. In this work, significant difference of ADC estimation between high b-values group and low b-values group has been shown in the healthy volunteer study ($p<0.05$ for all three sequences). On the contrary, there is no significant difference between two b-value groups in corrected diffusion coefficients from kurtosis model, with $p>0.1$ for all the three pulse sequences. This distinct behavior of the mono-exponential and kurtosis models may be due to the different effects of restricted diffusion or noise floor effects in the two diffusion models.

In addition to demonstrating reproducibility across pulse sequences, the quantitative diffusion measurements obtained in this study are in good agreement with previous works. In healthy young volunteers, ADC measurements with low b-value group ssEPI are $1.34\pm0.09\times10^{-3}$ mm^2/s in CG and $1.38\pm0.26\times10^{-3}$ mm^2/s in PZ. This agrees with the results from a previous prostate imaging study in young healthy subjects [25], where the ADC values are 1.22 (0.95-1.74) $\times10^{-3}$ mm^2/s in CG and 1.30 (1.21-2.08) $\times10^{-3}$ mm^2/s in PZ. In the patients, ADC values measured from ssEPI within CG (BPH not excluded) and healthy PZ were $1.29\pm0.17\times10^{-3}$ mm^2/s and $1.74\pm0.23\times10^{-3}$ mm^2/s, respectively. The results are in good agreement with previous measurements [9–11].

Overall, novel pulse sequences like rFOV and msEPI have been shown to be good alternatives to ssEPI for high quality diffusion-weighted images with less distortion. Also, they are both promising techniques for reproducible quantitative diffusion measurements compared to ssEPI and reproducible measurements across different acquisition parameters. However, rFOV and msEPI have different characteristics in terms of FOV, SNR and acquisition time. Therefore, in practice, the choice between rFOV and msEPI may be driven by the desired FOV, resolution and possible scan time constraints.

This study had several important limitations. In this work, rFOV and msEPI measurements are compared to ssEPI because there is no available gold standard reference for ADC in tissues (particularly in the presence of restricted diffusion). Further, an important motivation of this work was to assess whether previously derived quantitative criteria (e.g., relevant ADC thresholds derived using ssEPI [32–34]) can potentially be applicable to ADC measurements obtained using rFOV or msEPI. In addition, we optimized each sequence for performance, hence different spatial resolutions and readout directions were used for different pulse sequences. The different spatial resolutions may have effects on the visualization of edges or lesion in DWI, but it does not affect the ADC measurements as shown in the phantom results. Most importantly, only healthy tissues in the clinical patients were evaluated in the statistical analysis of this study. Based on the promising preliminary

data provided by this study in phantoms, healthy volunteers, and healthy tissues in patients, future clinical studies are needed to evaluate the ability of rFOV and msEPI to assess prostate cancer. Additionally, future studies will be needed to assess the reproducibility of diffusion measurements from rFOV and ssEPI at different field strengths, different coils, and using scanners from different vendors.

In conclusion, quantitative diffusion measurements demonstrate good reproducibility across diffusion MRI pulse sequences. Measurements from two novel sequences (rFOV and msEPI) with reduced image distortion are in good agreement with a standard ssEPI sequence. Therefore, both rFOV and msEPI have the potential to provide high image quality with reproducible quantitative diffusion measurements in prostate diffusion MRI.

Acknowledgments

The authors would like to thank Ed Jackson, PhD, for assistance with the phantom experiments. We also acknowledge research support from GE Healthcare. The authors acknowledge grant support from NIH-NIDDK Wisconsin Multidisciplinary K12 Urologic Research Career Development Program K12DK100022 (PD: D. Bjorling).

References

1. Padhani AR, Liu G, Mu-Koh D, Chenevert TL, Thoeny HC, Takahara T, Dzik-Jurasz A, Ross BD, Van Cauteren M, Collins D, et al. Diffusion-weighted magnetic resonance imaging as a cancer biomarker: consensus and recommendations. Neoplasia. 2009; 11:102–125. [PubMed: 19186405]
2. Jensen JH, Helpern JA, Ramani A, Lu H, Kaczynski K. Diffusional kurtosis imaging: The quantification of non-gaussian water diffusion by means of magnetic resonance imaging. Magnetic Resonance in Medicine. 2005; 53:1432–1440. [PubMed: 15906300]
3. Lu H, Jensen JH, Ramani A, Helpern JA. Three-dimensional characterization of non-gaussian water diffusion in humans using diffusion kurtosis imaging. NMR in Biomedicine. 2006; 19:236–247. [PubMed: 16521095]
4. Torre LA, Bray F, Siegel RL, Ferlay J, Lortet-Tieulent J, Jemal A. Global cancer statistics, 2012. CA: a cancer journal for clinicians. 2015; 65:87–108. [PubMed: 25651787]
5. Siegel RL, Miller KD, Jemal A. Cancer statistics, 2016. CA: a cancer journal for clinicians. 2016; 66:7–30. [PubMed: 26742998]
6. Smith RA, Manassaram-Baptiste D, Brooks D, Doroshenk M, Fedewa S, Saslow D, Brawley OW, Wender R. Cancer screening in the united states, 2015: A review of current american cancer society guidelines and current issues in cancer screening. CA: a cancer journal for clinicians. 2015; 65:30–54. [PubMed: 25581023]
7. Tan CH, Wang J, Kundra V. Diffusion weighted imaging in prostate cancer. European radiology. 2011; 21:593–603. [PubMed: 20936413]
8. Barentsz JO, Richenberg J, Clements R, Choyke P, Verma S, Villeirs G, Rouviere O, Logager V, Futterer JJ. ESUR prostate MR guidelines 2012. European radiology. 2012; 22:746–757. [PubMed: 22322308]
9. Gibbs P, Pickles MD, Turnbull LW. Diffusion imaging of the prostate at 3.0 Tesla. Investigative radiology. 2006; 41:185–188. [PubMed: 16428991]
10. Hosseinzadeh K, Schwarz SD. Endorectal diffusion-weighted imaging in prostate cancer to differentiate malignant and benign peripheral zone tissue. Journal of Magnetic Resonance Imaging. 2004; 20:654–661. [PubMed: 15390142]
11. Issa B. In vivo measurement of the apparent diffusion coefficient in normal and malignant prostatic tissues using echo-planar imaging. Journal of Magnetic Resonance Imaging. 2002; 16:196–200. [PubMed: 12203768]

12. Roethke MC, Kuder TA, Kuru TH, Fenchel M, Hadaschik BA, Laun FB, Schlemmer HP, Stieltjes B. Evaluation of diffusion kurtosis imaging versus standard diffusion imaging for detection and grading of peripheral zone prostate cancer. Investigative radiology. 2015; 50:483–489. [PubMed: 25867657]
13. Mazzoni LN, Lucarini S, Chiti S, Busoni S, Gori C, Menchi I. Diffusion-weighted signal models in healthy and cancerous peripheral prostate tissues: Comparison of outcomes obtained at different b-values. Journal of Magnetic Resonance Imaging. 2014; 39:512–518. [PubMed: 23723087]
14. Emine, S Ulku, Cunningham, CH., Jin Hyung, L., Han, ET., Nishimura, DG. DWI of the spinal cord with reduced FOV single-shot EPI. Magn Reson Med. 2008
15. Holdsworth SJ, Skare S, Newbould RD, Guzmann R, Blevins NH, Bammer R. Readout-segmented EPI for rapid high resolution diffusion imaging at 3T. European journal of radiology. 2008; 65:36–46. [PubMed: 17980534]
16. Porter DA, Heidemann RM. High resolution diffusion-weighted imaging using readout-segmented echo-planar imaging, parallel imaging and a two-dimensional navigator-based reacquisition. Magnetic resonance in medicine. 2009; 62:468–475. [PubMed: 19449372]
17. Nan-kuei C, Arnaud G, Hing-Chiu C, Song AW. A robust multi-shot scan strategy for high-resolution diffusion weighted MRI enabled by multiplexed sensitivity-encoding (MUSE). NeuroImage. 2013
18. Ohgiya Y, Suyama J, Seino N, Hashizume T, Kawahara M, Sai S, Saiki M, Munechika J, Hirose M, Gokan T. Diagnostic accuracy of ultra-high-b-value 3.0-t diffusion-weighted MR imaging for detection of prostate cancer. Clinical imaging. 2012; 36:526–531. [PubMed: 22920357]
19. Korn N, Kurhanewicz J, Banerjee S, Starobinets O, Saritas E, Noworolski S. Reduced-FOV excitation decreases susceptibility artifact in diffusion-weighted MRI with endorectal coil for prostate cancer detection. Magnetic resonance imaging. 2015; 33:56–62. [PubMed: 25200645]
20. Fedorov A, Tuncali K, Panych LP, Fairhurst J, Hassanzadeh E, Seethamraju RT, Tempany CM, Maier SE. Segmented diffusion-weighted imaging of the prostate: Application to transperineal in-bore 3T MR image-guided targeted biopsy. Magnetic resonance imaging. 2016; 34:1146–1154. [PubMed: 27240900]
21. Rabanillo, I., Holmes, JH., Guidon, A., Aja-Fernandez, S., Alberola-Lopez, C., Reeder, SB., Hernando, D. ADC measurement accuracy in quantitative diffusion phantoms using reduced field-of-view and multi-shot acquisitions. ISMRM Workshop on Breaking the Barriers of Diffusion MRI; 2016.
22. Banerjee I, Aramburu-Nunez D, Paudyal R, Chenevert T, Boss M, Shukla-Dave A. Does reduced FOV diffusion weighted imaging inherently yield lower ADC? 24th ISMRM. 2016
23. Pierpaoli C, Sarlls J, Nevo U, Basser P, Horkay F. Polyvinylpyrrolidone (PVP) water solutions as isotropic phantoms for diffusion MRI studies. In Proc Intl Soc Magn Reson Med. 2009; 17:1414.
24. Field A. Discovering statistics using IBM SPSS statistics. Sage. 2013
25. Medved M, Sammet S, Yousuf A, Oto A. MR imaging of the prostate and adjacent anatomic structures before, during, and after ejaculation: qualitative and quantitative evaluation. Radiology. 2014; 271:452–460. [PubMed: 24495265]
26. Scott AD, Nielles-Vallespin S, Ferreira PF, McGill LA, Pennell DJ, Firmin DN. The effects of noise in cardiac diffusion tensor imaging and the benefits of averaging complex data. NMR in Biomedicine. 2016; 29:588–599. [PubMed: 26891219]
27. Jones DK, Basser PJ. squashing peanuts and smashing pumpkins: How noise distorts diffusion-weighted MR data? Magnetic Resonance in Medicine. 2004; 52:979–993. [PubMed: 15508154]
28. Ma C, Li Y, Pan C, et al. High resolution diffusion weighted magnetic resonance imaging of the pancreas using reduced field of view single-shot echo-planar imaging at 3 T. Magnetic Resonance Imaging. 2014; 32(2):125–131. [PubMed: 24231348]
29. Zaharchuk G, Saritas EU, Andre JB, et al. Reduced field-of-view diffusion imaging of the human spinal cord: comparison with conventional single-shot echo-planar imaging. American Journal of Neuroradiology. 2011; 32(5):813–820. [PubMed: 21454408]
30. Lu Y, Hatzoglou V, Banerjee S, et al. Repeatability investigation of reduced field-of-view diffusion weighted magnetic resonance imaging on thyroid glands. Journal of computer assisted tomography. 2015; 39:334–339. [PubMed: 25700226]

31. Kim H, Lee JM, Yoon JH, et al. Reduced field-of-view diffusion-weighted magnetic resonance imaging of Pancreas: Comparison with conventional Single-Shot Echo-Planar imaging. Korean Journal of Radiology. 2015; 16:1216–1225. [PubMed: 26576110]
32. Vargas HA, Akin O, Franiel T, et al. Diffusion-weighted endorectal MR imaging at 3T for prostate cancer: Tumor detection and assessment of aggressiveness. Radiology. 2011; 259(3):775–784. [PubMed: 21436085]
33. Reischauer C, Froehlich JM, Koh DM, et al. Bone metastases from prostate cancer: assessing treatment response by using diffusion-weighted imaging and functional diffusion maps – initial observation 1. Radiology. 2010; 257(2):523–531. [PubMed: 20829534]
34. Thoeny HC, Ross BD. Predicting and monitoring cancer treatment response with diffusion-weighted MRI. Journal of Magnetic Resonance Imaging. 2010; 32(1):2–16. [PubMed: 20575076]
35. Thierfelder KM, Scherr MK, Notohamiprodjo M, Weiß J, Dietrich O, et al. Diffusion-weighted MRI of the prostate: advantages of zoomed EPI with parallel-transmit-accelerated 2d-selective excitation imaging. European Radiology. 2014; 24(12):3233–41. [PubMed: 25154727]
36. Barth BK, Cornelius A, Nanz D, Eberli D, Donati OF. Diffusion-weighted imaging of the prostate: image quality and geometric distortion of readout-segmented versus selective-excitation accelerated acquisitions. Investigative Radiology. 2015; 50(11):785. [PubMed: 26146870]
37. Rosenkrantz AB, Chandarana H, Pfeuffer J, Triolo MJ, Shaikh MB, Mossa DJ, et al. Zoomed echo-planar imaging using parallel transmission: impact on image quality of diffusion-weighted imaging of the prostate at 3T. Abdominal Radiology. 2015; 40(1):120–126.
38. D F Jr, Costa DN, Yuan Q, Rofsky NM, Lenkinski RE, Pedrosa I. Geometric distortion in diffusion-weighted MR imaging of the prostate-contributing factors and strategies for improvement. Academic Radiology. 2014; 21(6):817–23. [PubMed: 24709379]
39. Brendle C, Martirosian P, Schwenzer NF, Kaufmann S, Kruck S, Kramer U, et al. Diffusion-weighted imaging in the assessment of prostate cancer: comparison of zoomed imaging and conventional technique. European Journal of Radiology. 2016; 85(5):893–900. [PubMed: 27130048]
40. Giavarina D. Understanding Bland Altman analysis. Biochemia medica: Biochemia medica. 2015; 25(2):141–151. [PubMed: 26110027]
41. Tamura C, Shinmoto H, Soga S, Okamura T, Sato H, Okuaki T, et al. Diffusion kurtosis imaging study of prostate cancer: preliminary findings. Journal of Magnetic Resonance Imaging. 2014; 40(3):723–729. [PubMed: 24924835]
42. Suo S, Chen X, Wu L, Zhang X, Yao Q, et al. Non-Gaussian water diffusion kurtosis imaging of prostate cancer. Magnetic Resonance Imaging. 2014; 32(5):421–427. [PubMed: 24602826]
43. Rosenkrantz AB, Padhani AR, Chenevert TL, Koh DM, De Keyzer F, Taouli B, Le Bihan D. Body diffusion kurtosis imaging: basic principles, applications, and considerations for clinical practice. Journal of Magnetic Resonance Imaging. 2015; 42(5):1190–1202. [PubMed: 26119267]
44. Babourina-Brooks B, Cowin GJ, Wang D. Diffusion-weighted imaging in the prostate: an apparent diffusion coefficient comparison of half-Fourier acquisition single-shot turbo spin-echo and echo planar imaging. Magnetic Resonance Imaging. 2012; 30(2):189–194. [PubMed: 22055748]

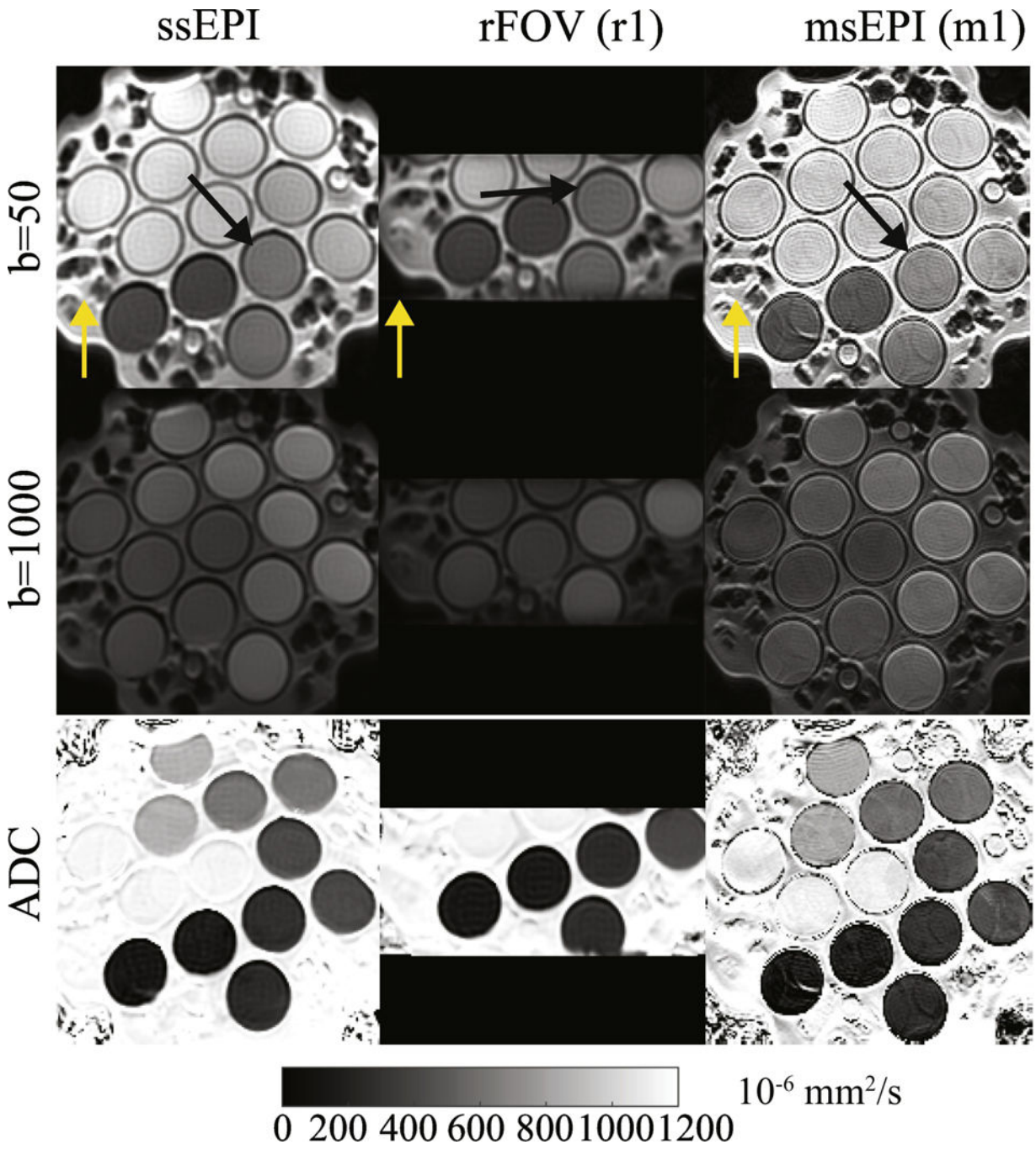

Figure 1.

Representative diffusion-weighted images and ADC maps across three sequences on a diffusion phantom. Black arrows indicate an area with distortions in ssEPI images. Yellow arrows for each sequence represent the phase encoding direction.

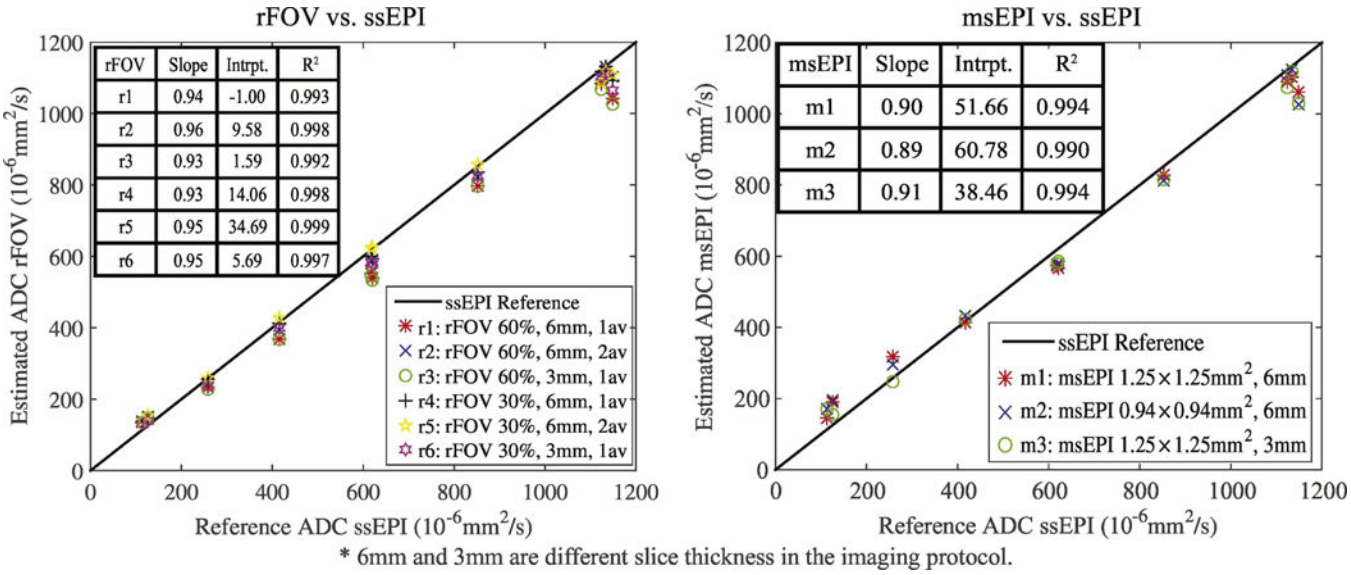

Figure 2.

Comparison between the averaged estimated ADC values from rFOV and msEPI and the reference ADC values from ssEPI within different vials of the diffusion phantom.

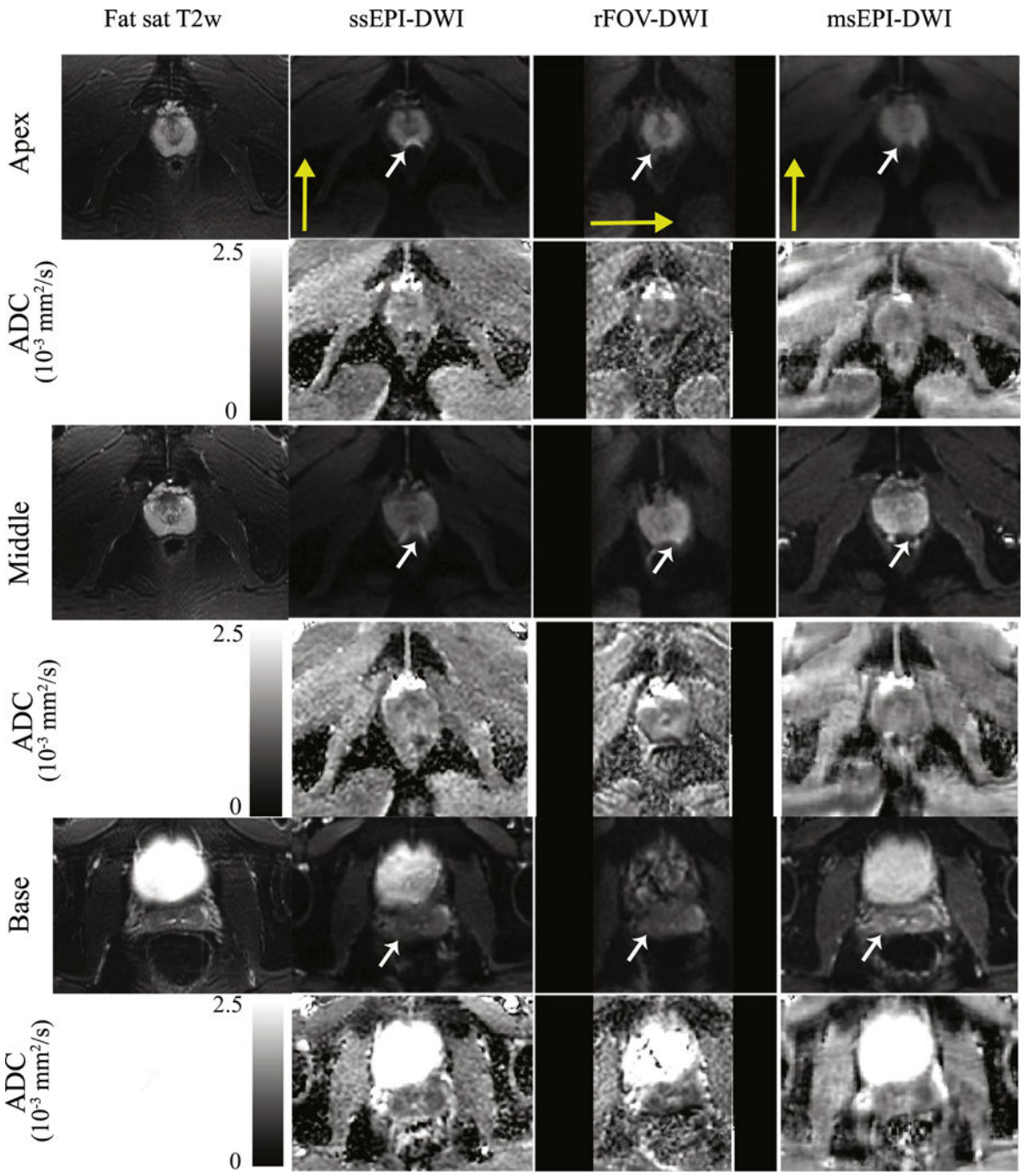

Figure 3.

Representative diffusion-weighted images and ADC maps across three sequences of a healthy volunteer. Three different slices from the apex, middle and base plane of the prostate respectively are shown with corresponding T2-weighted FSE images for illustration of the distortion. White arrows indicate an area with distortions in ssEPI images. Yellow arrows for each sequence represent the phase encoding direction.

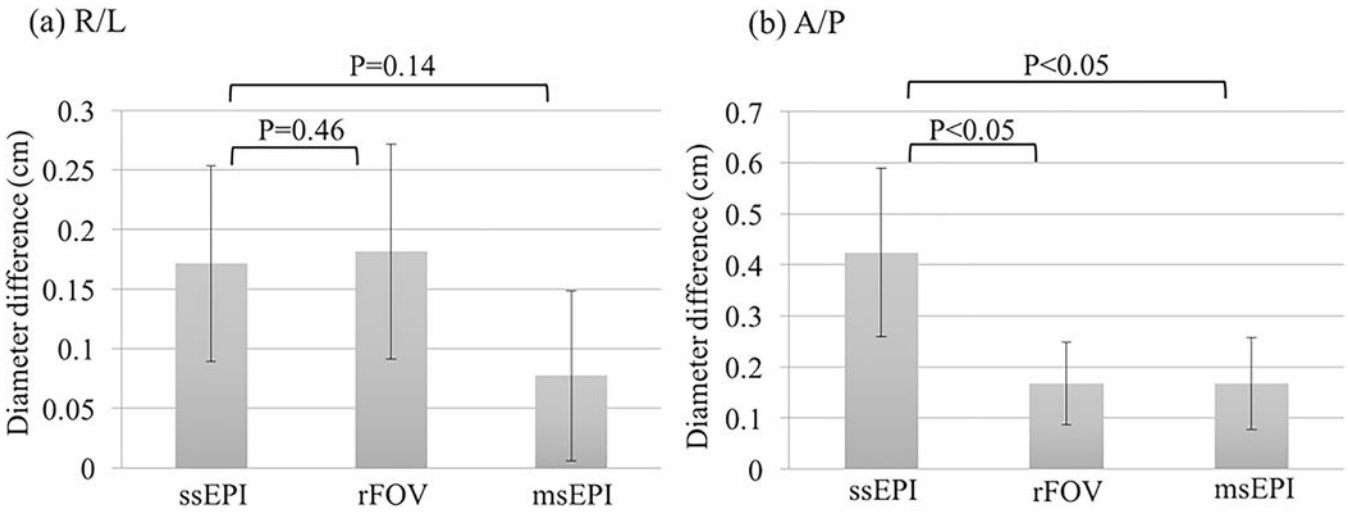

Figure 4.

Diameter differences in R/L and A/P directions between diffusion-weighted images from different sequences and an axial, non-EPI, T2-weighted acquisition (used as the reference). These diameter differences are evaluated as a measure of image distortion for each diffusion pulse sequence. P-values from t-test are shown for rFOV and msEPI compared to ssEPI, respectively.

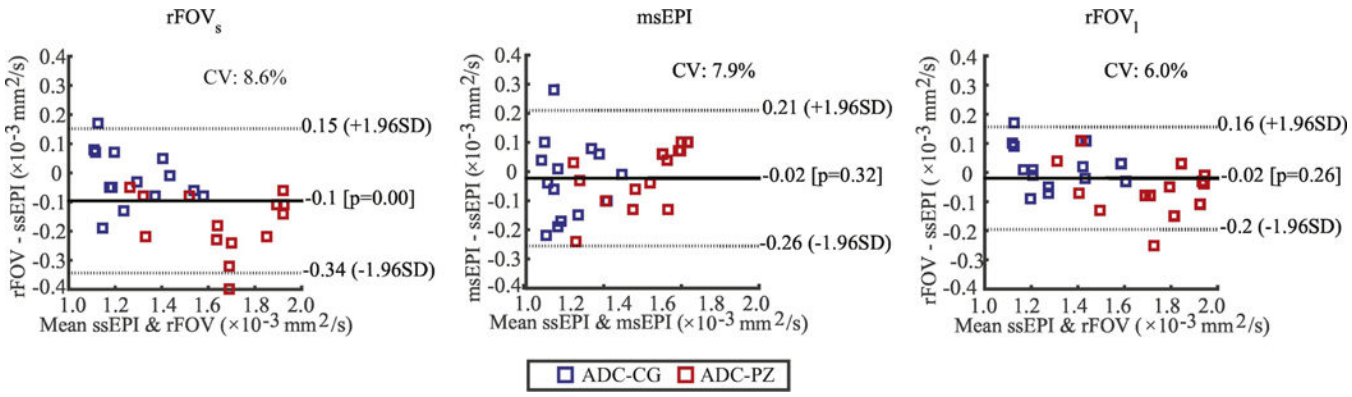

Figure 5.

Bland-Altman analysis of patient data. ADC measurements across different sequences (rFOV$_s$ versus ssEPI, msEPI versus ssEPI, and rFOV$_l$ versus ssEPI) were compared.

Table 1

Imaging protocols in diffusion phantom studies

	Sequence	FOV (cm^2)	In-plane Resolution (mm^2)	Slice Thickness (mm)	TE(ms)	TR(s)	b-values (s/mm^2)	Average	Diffusion direction
	ssEPI	24×24	1.9×1.9	6	86.3			1	
	msEPI(m1)	24×24	1.25×1.25	6	68.9			1	
	msEPI(m2)	24×24	0.94×0.94	6	70.0			1	
	msEPI(m3)	24×24	1.25×1.25	3	69.6			1	
3T scanner	rFOV(r1)	24×7.2	1.9×2.25	6	74.1	4	50,150,300 500,800,1000	1	All
	rFOV(r2)	24×7.2	1.9×2.25	6	74.1			[2]	
	rFOV(r3)	24×7.2	1.9×2.25	3	73.4			1	
	rFOV(r4)	24×14.4	1.9×2.88	6	73.9			1	
	rFOV(r5)	24×14.4	1.9×2.88	6	73.9			[2]	
	rFOV(r6)	24×14.4	1.9×2.88	3	73.1			1	

Table 2

Imaging protocols in prostate imaging studies

(a) Healthy volunteer studies

Sequence	FOV (cm^2)	In-plane Resolution (mm^2)	Slice Thickness/gap (mm)	TE (ms)	TR (s)	b-values * (s/mm^2)	Scan time
ssEPI	26×26	2.0×2.0	4/1	54.2	3	10(4),50(4),100(4),200(4), 400(16),600(16),800(16)	3min 21sec
	26×26	2.0×2.0	4/1	60.7	3	10(2),50(2),100(2),400(8), 800(8),1200(16),1500(16)	3min 57sec
rFOV	26×10.4	2.0×2.0	4/1	49.2	3	10(4),50(4),100(4),200(4), 400(16),600(16),800(16)	3min 21sec
	26×10.4	2.0×2.0	4/1	56.1	3	10(2),50(2),100(2),400(8), 800(8),1200(16),1500(16)	3min 57sec
msEPI	32×32	1.6×1.6	4/1	44.8	3	10(4),50(4),100(4),200(4), 400(16),600(16),800(16)	6min 48sec
	32×32	1.6×1.6	4/1	51.7	3	10(2),50(2),100(2),400(8), 800(8),1200(16),1500(16)	8min 48sec

(b) Patient studies

Sequence	FOV (cm^2)	In-plane Resolution (mm^2)	Slice Thickness/gap (mm)	TE (ms)	TR (s)	b-values (s/mm^2)	Scan time
ssEPI	24×24	2.0×2.0	4.8/0.2	67.1	4	100(1), 800(4)	1min 08sec
rFOVs	24×12	2.0×2.0	4.8/0.2	62.9	4	100(1), 800(4)	1min 08sec
rFOVl	24×12	2.0×2.0	4.8/0.2	63.5	4	100(6), 800(12)	4min 10sec
msEPI	32×32	1.6×1.6	4.8/0.2	56.9	4	100(1), 800(4)	4min 08sec

* Numbers in the brackets are the average numbers of each b-value

Table 3

Diffusion measurements of prostate imaging studies

(a) Diffusion measurements of healthy volunteers

Sequence	b-values group	Mono-exponential ADC×10^{-3}(mm^2/s)		Kurtosis D_k×10^{-3} (mm^2/s)		Kurtosis k	
		CG	PZ	CG	PZ	CG	PZ
ssEPI	Low	1.34±0.09	1.38±0.26	1.57±0.17	1.64±0.24	0.79±0.24	0.92±0.30
	High	1.24±0.09	1.29±0.27	1.59±0.17	1.68±0.31	0.76±0.10	0.81±0.16
rFOV	Low	1.33±0.09	1.39±0.15	1.59±0.18	1.67±0.22	0.86±0.36	0.85±0.37
	High	1.20±0.10	1.29±0.25	1.59±0.15	1.74±0.25	0.84±0.11	0.87±0.19
msEPI	Low	1.32±0.14	1.33±0.21	1.62±0.22	1.59±0.29	0.98±0.42	0.86±0.43
	High	1.23±0.14	1.24±0.22	1.53±0.23	1.57±0.24	0.70±0.15	0.76±0.12

(b) ADC measurements in patients (×10^{-3} mm^2/s)

Sequence	Central Gland (including BPH)	Healthy Peripheral Zone
ssEPI	1.29±0.17	1.74±0.23
rFOVs	1.27±0.15	1.58±0.22
rFOVl	1.31±0.16	1.68±0.21
msEPI	1.26±0.17	1.73±0.29

*CG: Central gland; PZ: Peripheral zone.

**Low b-values group is b = [10, 50, 100, 200, 400, 600, 800] s/mm^2;

High b-values group is b = [10, 50, 100, 400, 800, 1200, 1500] s/mm^2.

Table 4

Bland-Altman analysis of healthy volunteer studies

(a) Bland-Altman analysis across pulse sequences (Bias [95% confidence interval])

Models	Quantity	b-values group	rFOV vs. ssEPI		msEPI vs. ssEPI	
			Bias±1.96SD	p	Bias±1.96SD	p
Mono-exponential	ADC × 10^{-3} (mm^2/s)	Low b values	0.00 [−0.21, 0.22]	0.86	−0.03 [−0.22, 0.15]	0.12
		High b-values	−0.02 [−0.21, 0.18]	0.45	−0.03 [−0.28, 0.22]	0.30
Kurtosis	D_k ×10^{-3} (mm^2/s)	Low b-values	0.03 [−0.39, 0.44]	0.60	0.00 [−0.36, 0.37]	0.95
		High b-values	0.03 [−0.29, 0.35]	0.49	−0.09 [−0.58, 0.40]	0.13

(b) Bland-Altman analysis across b-value groups (Bias [95% confidence interval])

Models	Quantity	ssEPI		rFOV		msEPI	
		Low vs. High b-values		Low vs. High b-values		Low vs. High b-values	
		Bias±1.96SD	p	Bias±1.96SD	p	Bias±1.96SD	p
Mono-exponential	ADC × 10^{-3} (mm^2/s)	−0.09 [−0.26, 0.08]	0.00	−0.11 [0.33, 0.10]	0.00	−0.09 [−0.25, 0.07]	0.01
Kurtosis	D_k ×10^{-3} (mm^2/s)	0.03 [−0.32, 0.38]	0.43	0.03 [−0.35, 0.42]	0.46	−0.06 [−0.40, 0.29]	0.16

* Low b-values group is b = [10, 50, 100, 200, 400, 600, 800] s/mm^2;

High b-values group is b = [10, 50, 100, 400, 800, 1200, 1500] s/mm^2.